metals

MDPI

Article

Comparison on Hysteresis Loops and Dislocation Configurations in Fatigued Face-Centered Cubic Single Crystals

Zhibin Xing, Lingwei Kong, Lei Pang, Xu Liu, Kunyang Ma, Wenbo Wu and Peng Li *

Center for High Pressure Science, State Key Laboratory of Metastable Materials Science and Technology, Yanshan University, Qinhuangdao 066004, China
* Correspondence: pengli@ysu.edu.cn; Tel.: +86-335-8074631

Abstract: The aggregation and evolution of dislocations form different configurations, which are the preferred locations for fatigue crack initiation. To analyze the spatial distribution of the same dislocation configuration and the resulting configuration morphologies on different observation planes, several typical hysteresis loops and dislocation configurations in fatigued face-centered cubic single crystals with various orientations were compared. The crystal orientations of these specimens were determined by the electron back-scattering diffraction technique in a Cambridge S360 Scanning Electron Microscope. It is well known that dislocation ladder and wall structures, as well as patch and vein structures, are distributed on their respective observation planes, $(1\bar{2}1)$ and (111). These correspond to the point defect direction and line defect direction of dislocations, respectively. Therefore, the wall structures on the $(1\bar{2}1)$ and (111) planes consist of point defects and line defects, which can be defined as point walls and line walls, respectively. Furthermore, the walls on the $(1\bar{2}1)$ plane consist of Persistent Slip Band ladders connected with each other, corresponding to the formation of deformation bands. The evolution of dislocation patterns follows a process from patch to ladder and from vein to wall. The formation of labyrinths and dislocation cells originates from the activation of different secondary slip systems. In one word, it can help us better understand the physical nature of metal fatigue and failure by studying the distribution and evolution of different configurations.

Keywords: dislocation configurations; cyclic deformation; observed plane; FCC single crystals

Citation: Xing, Z.; Kong, L.; Pang, L.; Liu, X.; Ma, K.; Wu, W.; Li, P. Comparison on Hysteresis Loops and Dislocation Configurations in Fatigued Face-Centered Cubic Single Crystals. *Metals* **2024**, *14*, 1023. https://doi.org/10.3390/met14091023

Academic Editor: Eric Hug

Received: 15 July 2024
Revised: 29 August 2024
Accepted: 4 September 2024
Published: 7 September 2024

1. Introduction

By analyzing the same dislocation pattern of fatigued face-centered cubic (FCC) single crystals from different observation planes, the 3D characteristics of dislocation configurations will be better distinguished. For instance, the term "Persistent Slip Band" (PSB) is broadly used to describe various slip morphologies on crystal surfaces [1–5]. However, PSB is a general concept related to the persistent phenomena in fatigued FCC crystals [6–10]. When we observe the PSB on the $(1\bar{2}1)$ plane, we see a dislocation ladder structure, while when we observe the same PSB on the (111) plane, we see the dislocation wall structure. Both dislocation ladder and wall are the projection of the same dislocation configuration on different observation planes. Likewise, the patch and vein structures also originate from the same dislocation pattern. Essentially, they correspond to the results of the aggregation and evolution of dislocation points and dislocation lines, respectively. With a deeper understanding of the formation mechanisms of different dislocation configurations, more precise names have been adopted, such as PSB ladders [11,12], PSB walls [13], labyrinths [14,15] and cells [16,17].

The use of ambiguous terminology has led to confusion, with structures sometimes being incorrectly named. For example, the ladder structure has been called a wall, and the patch structure has been referred to as a vein, due to an unclear understanding of dislocation configurations. For clarity, we first distinguished between the various typical

dislocation configurations. All dislocation configurations were carefully observed using a Stereoscan 360 (S360) Scanning Electron Microscopy (SEM), Leica, Cambridge, UK and the electron channeling contrast (ECC) technique. ECC images are similar in appearance to transmission electron micrographs but have a lower resolution [18–21]. However, the ECC technique in SEM is particularly advantageous for observing fatigued dislocation patterns over larger areas, especially near grain boundaries, deformation bands, or fatigue cracks [22–26].

2. Experimental Procedures

Some bulk FCC single crystal plates with various orientations were firstly grown from electrolytic gold (Au), silver (Ag), copper (Cu) and aluminum (Al) of 99.999% purity by the Bridgman method. Secondly, fatigue specimens of 7 mm × 5 mm × 16 mm in gauge section and 54 mm in total length were made by an electrospark cutting machine. The stress axis orientation of the first group of Au, Ag, Cu and Al single crystals can be referred to as $[\bar{2}27]$, $[\bar{2}33]$, $[\bar{2}36]$ and $[\bar{1}11]$, respectively. The second group of the loading axes of Cu single crystals with specific orientations are parallel to the [001], [011], $[\bar{1}11]$ and $[\bar{1}39]$ orientations, respectively.

The crystal orientations of these specimens were determined by the electron backscattering diffraction (EBSD) technique with an accuracy of $\pm 2^{\circ}$ in a Cambridge S360 SEM. Cyclic deformation was performed under symmetric push-pull loading at room temperature in air using a Shimadzu, Kyoto, Japan servo-hydraulic testing machine. A triangular waveform signal with a frequency of 0.5 Hz was used for total strain control, with plastic strain limitation. The resolution and control precision of plastic strain were better than 10^{-5}. The peak loads in tension and compression, as well as the hysteresis loops, were automatically recorded by a computer until cyclic saturation was reached, which means that the peak stress becomes constant, and the cyclic saturated number was 5000 in this experiment. Origin software (https://www.originlab.com/) was used for data processing to plot the relationship curves between the plastic shear strain amplitude and shear stress after 1, 10, 100, 1000 and 5000 cycles. After the fatigue tests, all the fatigued specimens were carefully electro-polished, and the dislocation configurations beneath the surface were meticulously observed using the ECC technique in a Cambridge S360 SEM.

3. Results and Discussion

3.1. Comparison on Hysteresis Loops of FCC Single Crystals with Various Orientations

Figure 1 exhibits the hysteresis loops of various FCC single crystals. The $[\bar{2}27]$-oriented Au single crystal and the $[\bar{2}33]$-oriented Ag single crystal show similar hysteresis loops from the first cycle to the 5000th cycle, with their shear stress increasing with the number of cycles. That is primarily due to work hardening mechanisms, dislocation interactions and the formation of dislocation structures that resist further deformation. At cyclic saturation, the saturation stresses of the Au and Ag single crystals are 23.4 MPa and 20 MPa, respectively. In comparison, the $[\bar{2}36]$ Cu single crystal has a larger hysteresis loop area at cyclic saturation, with a saturated shear stress of approximately 26.9 MPa. Notably different from the Au, Ag and Cu single crystals, the $[\bar{1}11]$ Al single crystal exhibits a minimum saturation stress of only 8.5 MPa at high plastic strain amplitude. In addition to elements, the crystallographic orientation significantly impacts the hysteresis loop of FCC single crystals.

Figure 2 shows the hysteresis loops of fatigued Cu single crystals with classical orientations of [001], [011], $[\bar{1}11]$ and $[\bar{1}39]$. By comparison, it can be observed that after 5000 cycles, the hysteresis loops of [001] and $[\bar{1}11]$ Cu single crystals exhibit obvious cyclic hardening, while the hysteresis loops of [011] and $[\bar{1}39]$ Cu single crystals show cyclic saturation. If the degree of cyclic hardening is not severe, the value of plastic work will change little. However, in cases of strong cyclic hardening, the plastic work of the materials becomes complex. Under constant plastic strain amplitude control, when cyclic hardening occurs, the material must increase its stress, causing the hysteresis loop area to reduce in order

to maintain constant strain amplitude. However, Kaneko et al. [27] considered that in the saturation stage, the Bauschinger energy parameter should be sensitive to a cyclic hardening or softening rate rather than to the hysteresis loop shape. Therefore, the use of the Bauschinger energy parameter to evaluate the Bauschinger effect is meaningless. The plastic work decreases with cyclic hardening, suggesting that cyclic hardening will increase fatigue damage and decrease fatigue life. In addition, the Bauschinger effect in Cu single crystals exhibits varying degrees of orientation dependence. [001] and [$\bar{1}$11] Cu single crystals display a typical Bauschinger effect, which gradually weakens with increasing cycles. In contrast, the Bauschinger effect in the [011] and [$\bar{1}$39] Cu single crystals is not obvious.

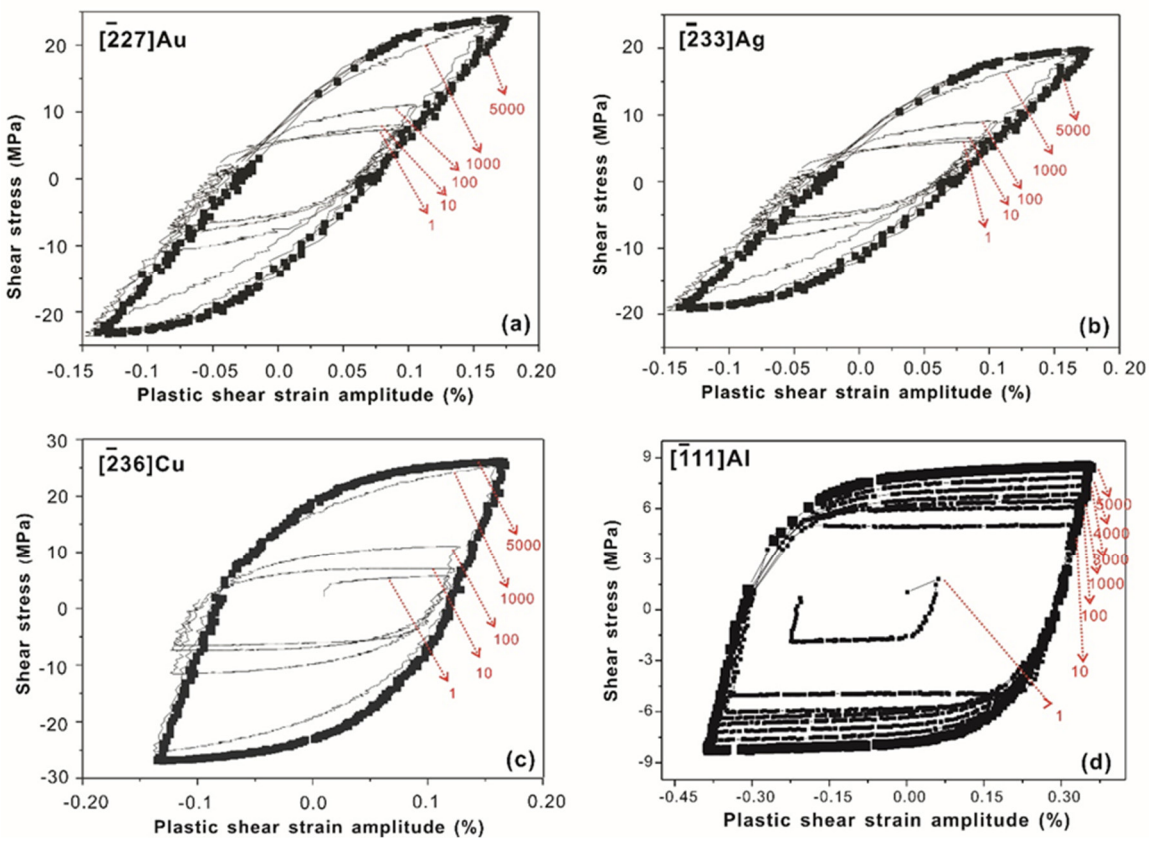

Figure 1. Comparison on the hysteresis loops of fatigued Au, Ag, Cu and Al single crystals. (**a**) [$\bar{2}$27]-oriented Au single crystal; (**b**) [$\bar{2}$33]-oriented Ag single crystal; (**c**) [$\bar{2}$36]-oriented Cu single crystal; (**d**) [$\bar{1}$11]-oriented Al single crystal.

3.2. Comparison between Dislocation Configurations: Patch vs. Vein and Ladder vs. Wall

Strictly speaking, veins and patches are not the same structure; they correspond to the PSB wall and PSB ladder structures, respectively. This difference arises from visual errors on different observation planes. Dislocations, being one-dimensional defects, appear differently depending on the observation direction. A dislocation may appear as a point or a line based on the chosen observation plane. Figure 3 illustrates the distinguishing features of veins and patches, ladders and walls. The primary slip system of FCC crystals is $(111)[\bar{1}01]$, and edge dislocations reciprocate along the $[\bar{1}01]$ direction, gradually converging and evolving to form the PSB ladder structure. These PSB ladders consist of point defects in dislocations and are best observed on the $(1\bar{2}1)$ plane. At the same time, on the (111) plane, PSB wall structures composed of dislocation line defects are visible. In an actual crystal, such ideal dislocation structures cannot be perfectly formed, but the overall trend holds true. The ladder structures on the $(1\bar{2}1)$ plane are equally spaced with the middle channel region containing numerous reciprocating screw dislocations [28]. Before forming

the ladder structure, crystals mainly consist of patches and channels in equal proportions, as shown in Figure 3a,b.

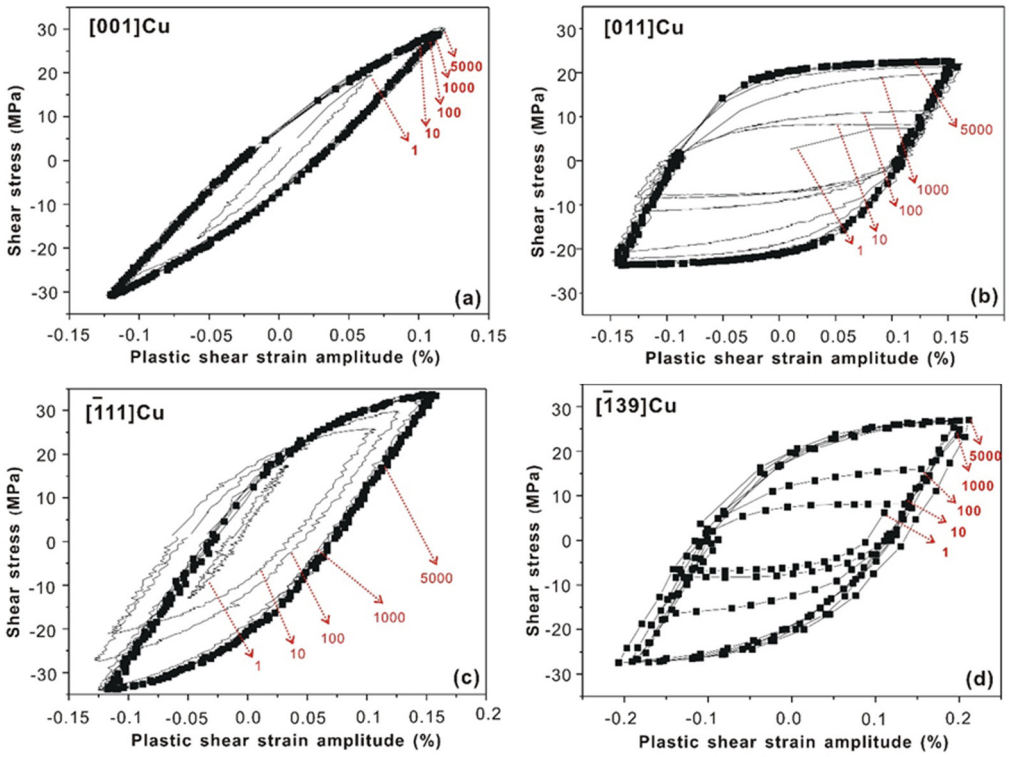

Figure 2. Comparison on the hysteresis loops of fatigued Cu single crystals with specific orientations. (**a**) [001]; (**b**) [011]; (**c**) [$\bar{1}$11]; (**d**) [$\bar{1}$39].

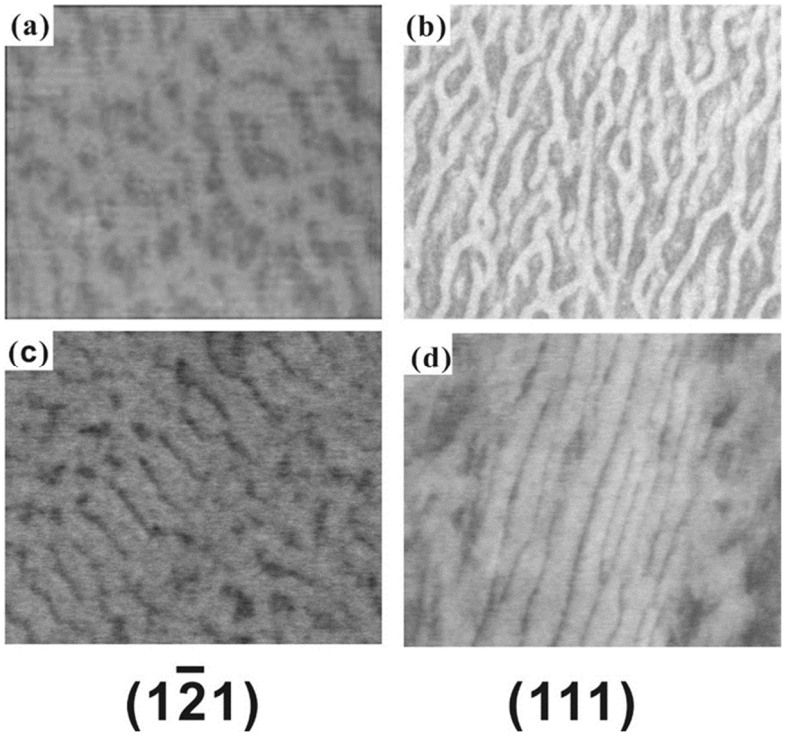

Figure 3. Dislocation configurations from different observed planes. (**a**,**c**) Patch and PSB ladder on plane (1$\bar{2}$1); (**b**,**d**) vein and wall on plane (111).

Therefore, patches and ladders exist on the $(1\bar{2}1)$ plane and correspond to each other. On the (111) plane, the patch structure formed by point defects is replaced by the vein structure formed by line defects. Thus, the patch and ladder structures are seen on the $(1\bar{2}1)$ plane, while the vein and wall structures are observed on the (111) plane. In essence, these structures are the same configurations viewed from different observation planes. Figure 4 presents a three-dimensional view of the dislocation configuration at saturation. As depicted, the $(1\bar{2}1)$ plane is mainly composed of a two-phase structure of patches and PSB ladders, while the vein structure is clearly visible on the (111) plane. Understanding these distinctions in observation planes is crucial to avoid confusion in dislocation configuration analysis.

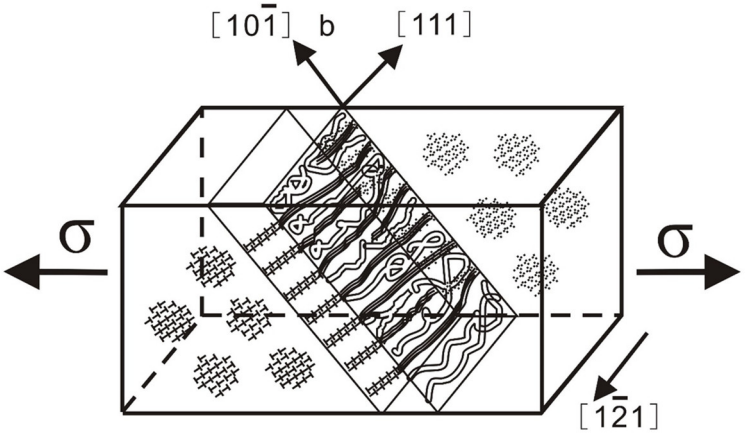

Figure 4. Three-dimensional comparison diagram of dislocation configurations: PSB ladder vs. wall and patch vs. vein.

3.3. Comparison between Wall Structures: Line Wall vs. Point Wall

Figure 5 systematically compares the differences between the (111) plane and the $(1\bar{2}1)$ plane wall structures. The wall structure on the (111) plane directly evolves from the matrix veins. It can be observed that the wall structure does not have the same length distribution as the ladder structure. In the wall structure, some walls may abruptly disappear, appearing as if only half remains. We refer to such walls as semi-atomic walls because they resemble the half-atomic planes caused by dislocations in the crystal, as clearly illustrated in Figure 5d. The wall structure on the $(1\bar{2}1)$ plane results from the further evolution of the PSB ladder structure in deformation band II (DBII). Zhang et al. [13] analyzed the transformation process of the PSB ladder to the wall structure in DBII. In a single-slip-oriented crystal, when the strain amplitude is high, besides the labyrinth or cell structures caused by the secondary slip system, a DBII composed of a PSB ladder or wall structure may form. Sometimes, due to orientation, no secondary slip system initiates even at higher strain amplitudes. When the strain has accumulated to a certain extent, the crystal must adjust the existing two-phase structure to bear higher plastic strain. This adjustment results in a sudden increase in the density of the slip zone in many local regions, forming DBII in the surface slip morphology.

At this stage, the DBII is still composed of the PSB ladder structure but accommodates greater plastic strain, termed a developing deformation band. These developing deformation bands are not final stable structures. The PSB ladders within them will repeatedly move under shear stress and gradually merge to form a developed deformation band composed of wall structures. From the above analysis, we understand that the formation of DBII is based on the full development of the slip band. Among the DBII and microscopic dislocation structures observed, more are composed of the PSB ladder or wall structure formed by the main slip system. Therefore, it is believed that the failure of the secondary slip system to initiate in time forces the crystal to adjust its distribution to adapt to the applied strain.

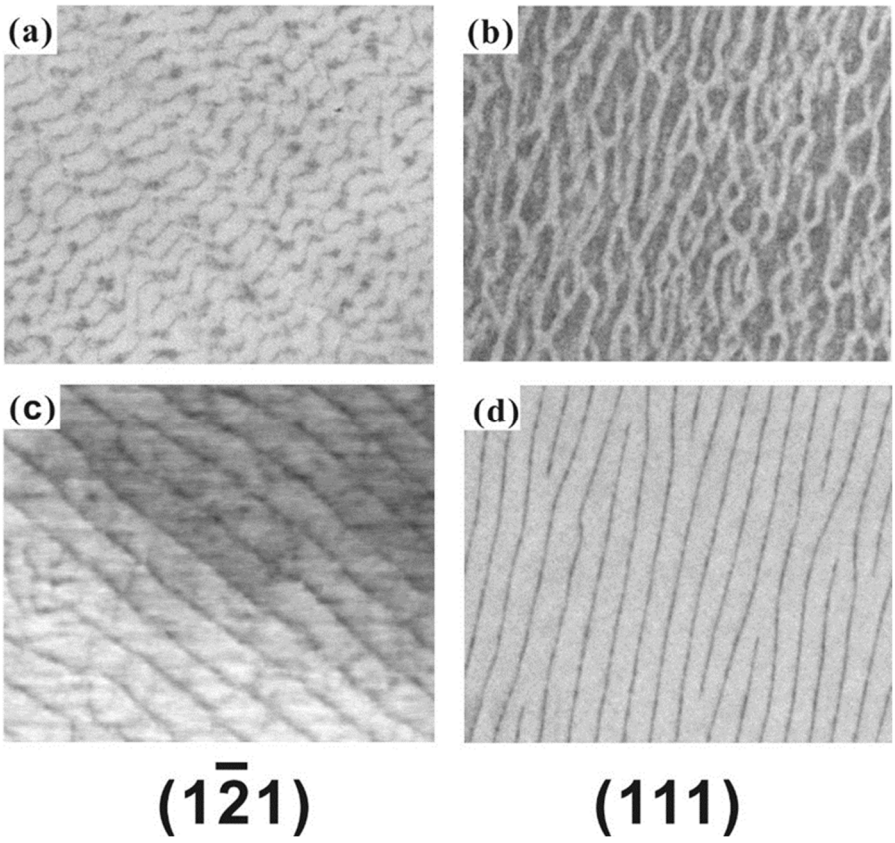

Figure 5. Dislocation configurations from different observed planes. (**a**,**c**) PSB ladder and PSB wall on plane $(1\bar{2}1)$; (**b**,**d**) vein and wall on plane (111).

So, what is the specific formation process of the wall structure in DBII? First, the slip system of the FCC crystal is $(111)[\bar{1}01]$. Based on the orientation relationship between the loading axis and the slip system, the shear stress of the randomly oriented crystal along the sliding direction can be determined as follows:

$$\tau_a = \sigma cos\varphi cos\phi = \Omega\sigma \quad (1)$$

In this formula, ϕ is the angle between the loading axis and the normal stress; φ denotes the angle between the loading axis and the slip direction; ϕ is the angle between the loading axis and the normal of the $(1\bar{2}1)$ observed plane; and Ω denotes the orientation factor. Secondly, DBII's habitus system is $(\bar{1}01)[111]$, conjugated to the slip system. Based on the orientation relationship between the loading axis and the habituation system, the shear stress of the randomly oriented crystal along the habit direction can be obtained as shown below:

$$\tau_b = \sigma cos\phi cos\varphi = \Omega\sigma \quad (2)$$

Compared with Equation (1), $\tau_{DBII} = \tau_b = \tau_a = \tau_{SB}$. In the case of FCC crystals, the applied stresses of the $(111)[\bar{1}01]$ and $(\bar{1}01)[111]$ systems are the same under axial load. However, the crystal will first choose $(111)[\bar{1}01]$ as the main slip system because it encounters the least lattice resistance along the most closely packed directions and planes of atoms [29]. Essentially, the crystal structure plays a decisive role. Following this idea, the formation process of the wall structure in DBII can be envisaged as follows. Under the action of the shear stress τ_a, the crystal begins to slide along the slip plane (111). As the cyclic deformation progresses, the dislocations continue to converge and form a regular dislocation configuration–PSB ladder structure, which corresponds to the plateau area in the cyclic stress–strain (CSS) curve. If the strain amplitude is further increased, a single resident slip zone will not be able to accommodate the larger plastic deformation. In such cases, the

crystal often forms a labyrinth or cell structure through the activation of the secondary slip system, corresponding to the C zone of the CSS curve. However, sometimes the secondary slip system does not activate in time, particularly in local areas. In these instances, the crystal undergoes plastic deformation in another manner—forming a deformation band. During this evolution process, the slip bands in the deformation zone are densely arranged, causing the ladder structures within these slip bands to reciprocate along the slip plane. Under the action of the shear stress τ_b, at certain moments, the dislocation ladders connect to form a shear plane. Along DBII's habitual plane $(\bar{1}01)$, the shear strain γ_b is generated, leading to the formation of the dislocation wall structure.

The results of Zhang et al. [13] show that DBII indeed accommodates a larger plastic deformation compared to the slip zone. Based on the volume fraction of DBII, they roughly estimate this amount of deformation to be between 7.5×10^{-3} and 2×10^{-2}. Additionally, the intrusion and extrusion caused by DBII are more intense than those caused by the slip bands. This is consistent with the formation process of the wall structure in DBII.

On the other hand, what is the difference between the wall structure observed from the $(1\bar{2}1)$ side and the traditional wall structure observed from the (111) side, apart from the observation plane?

To answer this question, let us first examine a set of pictures. Figure 6 shows two configurations consisting of points and lines, analogous to the ladder structure on the $(1\bar{2}1)$ side and the wall structure on the (111) side, respectively. When these two configurations are reduced to a certain scale, it becomes impossible to distinguish whether they consist of points or lines, which is similar to what we encounter when observing the dislocation configurations in FCC crystals. Although the configurations of dislocations are point defects and line defects, resulting from different observation plane selections, it becomes challenging to distinguish between the ladder structure and the wall structure. Similarly, the wall structure on the $(1\bar{2}1)$ side is also different from the wall structure on the (111) side.

Figure 6. Different profiles of dislocation and the formation of dislocation patterns. (**a**,**c**) Point defect and PSB ladder on plane $(1\bar{2}1)$; (**b**,**d**) line defect and PSB wall on plane (111).

3.4. Relationship between Dislocation Configurations: Vein vs. Wall and Labyrinth vs. Cell

So far, we have a clear understanding of the PSB ladder and PSB wall structures, and the same principle applies to distinguishing between patch structures and vein structures. Next, let us examine the relationship between vein and wall structures. Figure 7 presents a set of shaded images depicting the two-phase structure of veins and walls. Figure 7b shows the result of properly processing the vein structure on the right side of the PSB wall. By attempting to leave only the dislocations at the junction of the vein and the channel, and removing the dislocations at the core of the vein, we can see that the vein portion has been transformed into a structure similar to the PSB wall. Figure 7c,d highlight the image

contrast between wall and vein structures in two different ways. Although these images cannot serve as direct evidence, they reflect the internal relationship between veins and walls, as well as patches and ladders. We know that the wall structure results from the evolution of veins, where the dislocation-dense areas are further compressed. Figure 7 supports this reasonable judgment.

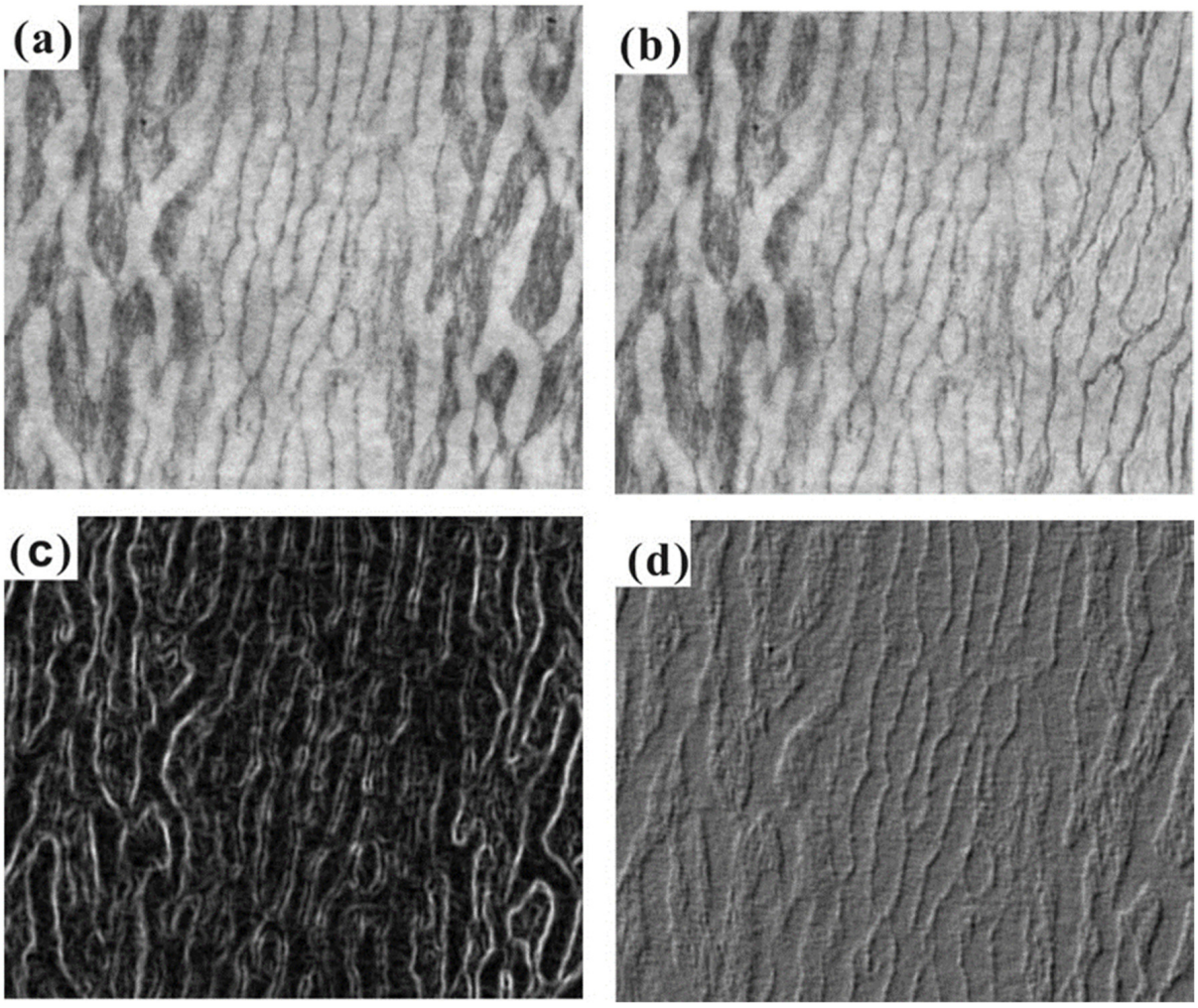

Figure 7. Relationship between vein and wall structures. (**a**) Vein and wall structures on plane (111); (**b**–**d**) different profiles of vein and wall structures.

Finally, let us discuss the relationship between the labyrinth and cell structures. Figure 8 shows two typical dislocation configurations on different observed planes, $(1\bar{2}1)$ and (111) [25]. The formation of labyrinth and cell structures results from secondary slip, with the specific activated slip system being the differentiating factor. The labyrinth structure forms due to the interaction of conjugate slip systems, while the cell structure derives from coplanar dislocation reactions, corresponding to Figure 8a,d, respectively. A detailed explanation will be provided in future studies. Here, we cautiously suggest that labyrinth structures observed from different planes do not follow the same reaction pattern, meaning that their composition is not identical, even though they may appear similar. The same applies to cell structures. For example, the labyrinth structure in Figure 8b should be reflected in the same section of two sets of slip systems, while the cell structure in Figure 8c is more likely a result of severe cross-slip. The latter two do not involve dislocation reactions and thus do not share the same formation mechanism as the previous labyrinth or cell structures.

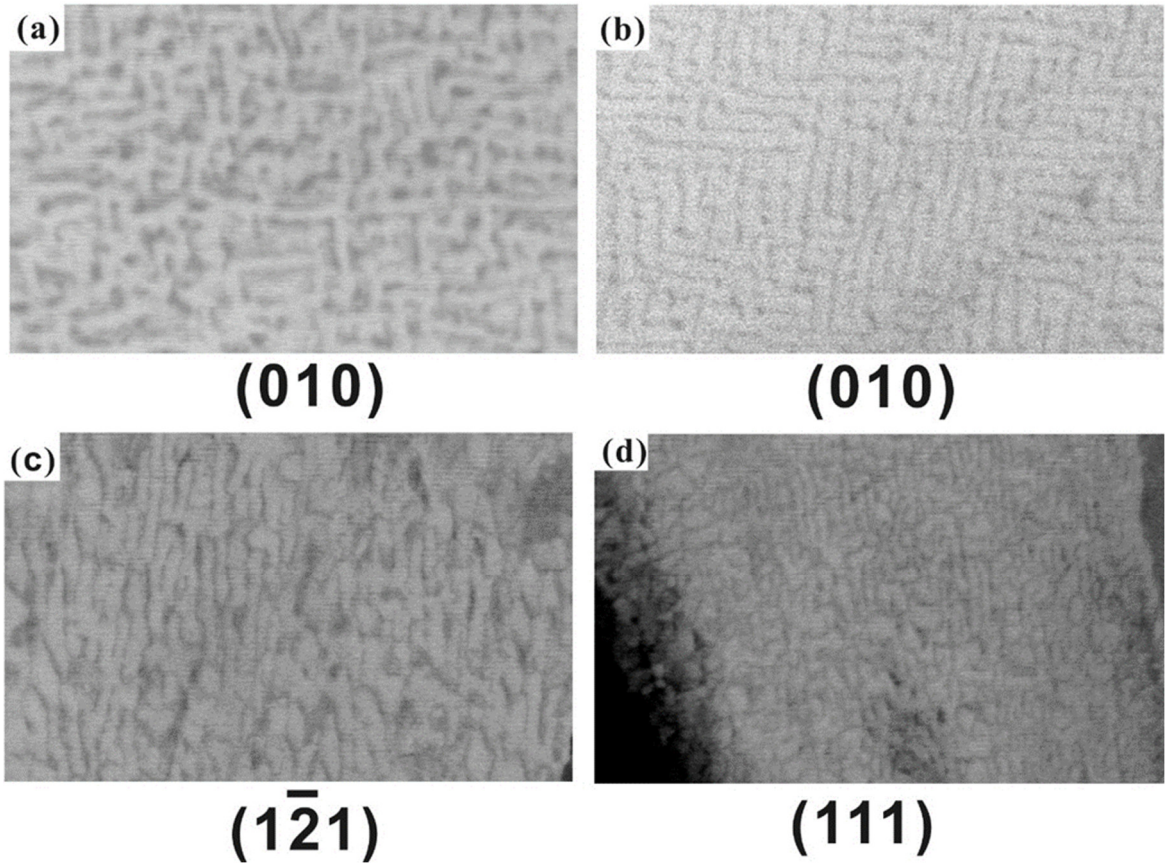

Figure 8. Dislocation configurations from different observed planes. (**a**,**c**) Labyrinth and cell structures on plane $(1\bar{2}1)$; (**b**,**d**) labyrinth and cell structures on plane (111).

4. Conclusions

To better understand the interrelationships among various dislocation configurations such as vein and patch, dislocation ladder and wall, labyrinth and cell structures, we compared different typical dislocation structures and examined the same structure on different observed planes, coming to the following conclusions:

1. The hysteresis loops of $[001]$ and $[\bar{1}11]$ Cu single crystals exhibit obvious cyclic hardening, while the hysteresis loops of $[011]$ and $[\bar{1}39]$ Cu single crystals show cyclic saturation. Additionally, the Bauschinger effect of Cu single crystals also exhibits orientation dependence.
2. Dislocation ladder and wall structure, as well as patch and vein structure, belong to their respective observation planes, $(1\bar{2}1)$ and (111), which correspond to point defects and line defects of dislocations, respectively.
3. The wall structures on the $(1\bar{2}1)$ and (111) planes are derived from the evolution of different dislocation configurations. This is because DBII, composed of wall structures, is prone to occur in $[011]$-oriented crystals. Due to having the largest angle between $[011]$ and $(\bar{1}01)$ in the stereographic triangles, only DBII with a $(\bar{1}01)$ habit plane can obtain the maximum nucleation driving force.
4. The change in dislocation density between the vein and the wall indicates that the wall structure is the result of the evolution of the veins, with dislocation-intensive areas becoming further compressed. The formation of labyrinth and cell structures implies the activation of different slip systems. In summary, the dislocation configuration is a three-dimensional structure, with each section observed on different planes representing only a part of the whole structure.

Author Contributions: Conceptualization, P.L.; methodology, Z.X., L.P. and X.L.; validation, P.L., Z.X. and L.K.; formal analysis, P.L. and Z.X.; investigation, Z.X., L.K., K.M. and W.W.; resources, Z.X., L.K., L.P. and X.L.; data curation, K.M. and W.W.; writing—original draft preparation, Z.X.; writing—review and editing, P.L.; supervision, P.L.; project administration, P.L.; funding acquisition, P.L. All authors have read and agreed to the published version of the manuscript.

Funding: This work was financially supported by the National Natural Science Foundation of China (NSFC) under Grant Nos. 52288102 and 92163215, the 100 Talents Plan of Hebei Province under Grant No. E2020100005 and the Natural Science Foundation of Hebei Province under Grant No. E2022203109.

Data Availability Statement: The original contributions presented in the study are included in the article, and further inquiries can be directed to the corresponding author.

Acknowledgments: The authors acknowledge Z.F. Zhang and S.X. Li for their valuable suggestions and advice. Thanks are also due to H.H. Su, W. Gao, Q.Q. Duan and L.X. Zhang for their assistance in conducting the fatigue experiments and observing dislocation configurations.

Conflicts of Interest: The authors declare no conflicts of interest.

References

1. Thompson, N.B.W.; Wadsworth, N.J.; Louat, N. The origin of fatigue fracture in copper. *Philos. Mag.* **1956**, *1*, 113–126. [CrossRef]
2. Li, P.; Kong, L.W.; Zhang, Z.X.; Zhao, J.; Du, C.C.; Huang, J.Y.; Zhang, Z.F. In-situ TEM investigation of structural transformation from LEDS to twin in fatigued Cu single crystal during annealing. *Philos. Mag.* **2020**, *100*, 3070–3091. [CrossRef]
3. Yang, H.; Zhu, L.; Zhang, R.; Zhou, J.; Sun, Z. Shearing dominated by the coupling of the interfacial misfit and atomic bonding at the FCC (111) semi-coherent interfaces. *Mater. Design* **2020**, *186*, 108294. [CrossRef]
4. Lavenstein, S.; Gu, Y.; Madisetti, D.; El-Awady, J.A. The heterogeneity of persistent slip band nucleation and evolution in metals at the micrometer scale. *Science* **2020**, *370*, eabb2690. [CrossRef] [PubMed]
5. Meng, F.; Ferrié, E.; Déprés, C.; Fivel, M. 3D discrete dislocation dynamic investigations of persistent slip band formation in FCC metals under cyclical deformation. *Int. J. Fatigue* **2021**, *149*, 106234. [CrossRef]
6. Wang, X.; Zhao, Y.; Wang, L.; Wei, L.; He, J.; Guan, X. In-situ SEM investigation and modeling of small crack growth behavior of additively manufactured titanium alloy. *Int. J. Fatigue* **2021**, *149*, 106303. [CrossRef]
7. Dodaran, M.S.; Muhammad, M.; Shamsaei, N.; Shao, S. Synergistic effect of microstructure and defects on the initiation of fatigue cracks in additively manufactured Inconel 718. *Int. J. Fatigue* **2022**, *162*, 107002. [CrossRef]
8. Polák, J. Role of Persistent Slip Bands and Persistent Slip Markings in Fatigue Crack Initiation in Polycrystals. *Crystals* **2023**, *13*, 220. [CrossRef]
9. Babinský, T.; Kuběna, I.; Šulák, I.; Kruml, T.; Tobiáš, J.; Polák, J. Surface relief evolution and fatigue crack initiation in René 41 superalloy cycled at room temperature. *Mater. Sci. Eng. A* **2021**, *819*, 141520. [CrossRef]
10. Polák, J.; Man, J.; Kruml, T. The sources of cyclic slip irreversibility. *Acta Mater.* **2024**, *267*, 119709. [CrossRef]
11. Mughrabi, H. The cyclic hardening and saturation behaviour of copper single crystals. *Mat. Sci. Eng.* **1978**, *33*, 207–223. [CrossRef]
12. Winter, A.T. A model for the fatigue of copper at low plastic strain amplitudes. *Philos. Mag. A J. Theor. Exp. Appl. Phys.* **1974**, *30*, 719–738. [CrossRef]
13. Zhang, Z.F.; Wang, Z.G.; Sun, Z.M. Evolution and microstructural characteristics of deformation bands in fatigued copper single crystals. *Acta Mater.* **2001**, *49*, 2875–2886. [CrossRef]
14. Loretto, M.H. *Dislocations and Properties of Real Materials*; The Institute of Metals: London, UK, 1985.
15. Fujii, T.; Kajita, T.; Miyazawa, T.; Arai, S. Characterization of dislocation microstructures in cyclically deformed [001] copper single crystals using high voltage scanning transmission electron microscopy. *Mater. Charact.* **2018**, *136*, 206–211. [CrossRef]
16. Lepinoux, J.; Kubin, L.P. In situ TEM observations of the cyclic dislocation behaviour in persistent slip bands of copper single crystals. *Philos. Mag. A* **1985**, *51*, 675–696. [CrossRef]
17. Laird, C.; Wang, Z.; Ma, B.T.; Chai, H.F. Low energy dislocation structures produced by cyclic softening. *Mater. Sci. Eng. A* **1989**, *113*, 245–257. [CrossRef]
18. Zauter, R.; Petry, F.; Bayerlein, M.; Sommer, C.; Christ, H.J.; Mughrabi, H. Electron channelling contrast as a supplementary method for microstructural investigations in deformed metals. *Philos. Mag. A* **1992**, *66*, 425–436. [CrossRef]
19. Schwab, A.; Bretschneider, J.; Buque, C.; Blochwitz, C.; Holste, C. Application of electron channelling contrast to the investigation of strain localization effects in cyclically deformed fcc crystals. *Phil. Mag. Lett.* **1996**, *74*, 449–454. [CrossRef]
20. Melisova, D.; Weiss, B.; Stickler, R. Nucleation of persistent slip bands in Cu single crystals under stress controlled cycling. *Scripta Mater.* **1997**, *36*, 1061–1066. [CrossRef]
21. Ahmed, J.; Wilkinson, A.J.; Roberts, S.G. Electron channelling contrast imaging characterization of dislocation structures associated with extrusion and intrusion systems and fatigue cracks in copper single crystals. *Philos. Mag. A* **2001**, *81*, 1473–1488. [CrossRef]
22. Zhang, Z.F.; Wang, Z.G. Investigations of dislocation patterns within grains and near grain boundaries in copper by the electron channelling contrast technique in scanning electron microscopy. *Phil. Mag. Lett.* **1998**, *78*, 105–113. [CrossRef]

23. Zhang, Z.F.; Wang, Z.G.; Hu, Y.M. Effects of grain boundary on slip morphology and dislocation patterns in a fatigued copper bicrystal. *Scripta Mater.* **1999**, *40*, 1353–1358. [CrossRef]
24. Zhang, Z.F.; Wang, Z.G. Dependence of intergranular fatigue cracking on the interactions of persistent slip bands with grain boundaries. *Acta Mater.* **2003**, *51*, 347–364. [CrossRef]
25. Li, S.X.; Li, X.W.; Zhang, Z.F.; Wang, Z.G.; Lu, K. On the formation of deformation bands in fatigued copper single crystals. *Philos. Mag. A* **2002**, *82*, 3129–3147. [CrossRef]
26. Vermeij, T.; Peerlings, R.H.J.; Geers, M.G.D.; Hoefnagels, J.P.M. Automated identification of slip system activity fields from digital image correlation data. *Acta Mater.* **2023**, *243*, 118502. [CrossRef]
27. Kaneko, Y.; Ishikawa, N.; Vinogradov, A.; Kitagawa, K. Hysteresis Loop Shape of a Cyclically-Deformed Copper Tricrystal Having Two Longitudinal Grain Boundaries. *Scripta Mater.* **1998**, *38*, 1609–1614. [CrossRef]
28. Wang, Q.; Wang, Q.; Gong, X.; Wang, T.; Zhang, W.; Li, L.; Liu, Y.; He, C.; Wang, C.; Zhang, H. A comparative study of low cycle fatigue behavior and microstructure of Cr-based steel at room and high temperatures. *Mater. Design* **2020**, *195*, 109000. [CrossRef]
29. Hou, J.P.; Wang, Q.; Zhang, Z.J.; Tian, Y.Z.; Wu, X.M.; Yang, H.J.; Li, X.W.; Zhang, Z.F. Nano-scale precipitates: The key to high strength and high conductivity in Al alloy wire. *Mater. Design* **2017**, *132*, 148–157. [CrossRef]